Deciphering TrFE Fingerprints in P(VDF-TrFE) by Raman Spectroscopy: Defect Quantification and Morphotropic Phase Boundary

Pedro Resende, Jean-David Isasa, Georges Hadziioannou, Guillaume Fleury

Deciphering TrFE Fingerprints in P(VDF-TrFE) by Raman Spectroscopy: Defect Quantification and Morphotropic Phase Boundary

Pedro M. Resende, Jean-David Isasa, Georges Hadziioannou, Guillaume Fleury*

Univ. Bordeaux, CNRS, Bordeaux INP, LCPO, UMR 5629, F-33600, Pessac, France

Keywords: Raman Spectroscopy, P(VDF-TrFE), Chain Conformation, Ferroelectric, Relaxor.

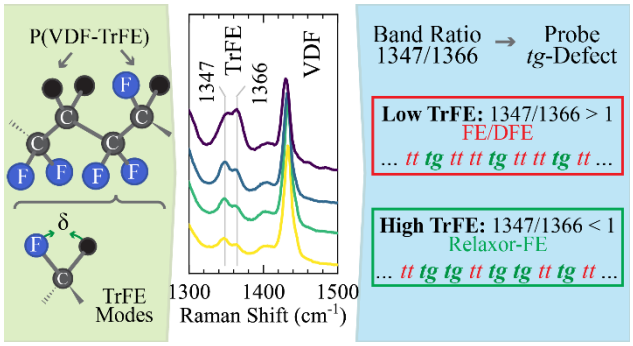

ABSTRACT:

The electroactive behavior of PVDF-based polymers is tightly related to the macromolecular sequence, chain conformation, and crystallinity. Although β-PVDF is the most attractive phase for applications in organic electronics, PVDF tends to crystallize into other thermodynamically more stable phases. Copolymerization of VDF and TrFE addressed this issue, and has resulted in high ferroelectric content co-polymers. Later on, the insertion of CFE/CTFE units into the P(VDF-TrFE) architecture yielded ter-polymers with relaxor-ferroelectric properties, especially attractive in energy storage and electrocaloric applications. The investigation of the corresponding electroactive phases in these polymers relied mainly on FT-IR and X-ray diffraction techniques, demanding an extensive combination of material characterization and analysis to detect the majority phases and predict material behavior. In this work, we demonstrate a facile and non-invasive approach to assess the relative ratio of defects in TrFE-

segments through a detailed analysis of the polymer Raman spectra. By varying the content of TrFE in P(VDF-TrFE) samples, a detailed assignation of the TrFE unit modes (1347 and 1366 cm^{-1}) contribution to the polymer Raman spectra was established which was further validated by FT-IR, X-ray diffraction, calorimetry, and dielectric spectroscopy measurements. Based on our findings, we further propose a defect quantification ratio that can be used to predict chain conformation and electroactive behavior.

INTRODUCTION

Poly(vinylidene fluoride)-based (PVDF) polymers have attractive ferrotronic properties, resulting in numerous applications in organic electronics: sensors and transducers (from piezo- and pyroelectricity); FETs for non-volatile memories (from ferroelectricity); energy harvesting from motion and temperature (piezo- and pyroelectricity, and electrocalorics); capacitors for energy storage (from relaxor-ferroelectric); and cooling applications (from electrocalorics).[1-11] The ferrotronic properties (ferro-, piezo-, pyro-electric and electrocaloric) of these materials are tightly related to their chain structure, and there are numerous reports investigating how these properties evolve as a function of processing and material composition.

PVDF is a polymorph that can crystallize into three main distinct phases: α (*tgtg'*), β (all-*trans*), and γ (*tttgtttg'*) phases. The α phase is paraelectric (PE) due to the anti-parallel orientation of adjacent chains (symmetric with respect to the *b* axis), having a net zero dipolar moment. In the β phase, adjacent chains are aligned parallel to each other, creating a non-zero dipolar moment along the *b* axis, at the origin of the ferroelectric (FE) behavior. The all-*trans* chain conformation maximizes the dipolar moment, as all the dipolar moments are aligned in the same direction. Finally, in the γ phase the polymer presents a non-zero dipolar moment, but much weaker than in the previous case. Additional phases are mentioned in the literature, which

correspond to variants of the α and γ phases. These phases present the same crystalline structures, but differ in the parallel or anti-parallel orientation of adjacent chains. PVDF predominantly crystallizes into the non-polar α phase requiring additional processing to obtain β phase. Different approaches have been demonstrated to successfully produce high β phase content, such as thermal annealing, material poling, film stretching, blending, or co-polymerization.[12-16] The last led to the development of co-polymers based on VDF and trifluoroethylene (TrFE) units, that readily crystallize into the β phase. Further research resulted in the observation of relaxor-ferroelectric (RFE) properties in electron-irradiated P(VDF-TrFE), explained by the local disruption of FE domains that softened FE hysteresis and lowered the remnant field.[17, 18] This is especially attractive for energy storage applications, providing a narrow material hysteresis with lower dielectric losses. RFE behavior was then obtained with P(VDF-TrFE) based ter-polymers by the addition of chlorofuoroethylene (CFE) or chlorotrifluoroethylene (CTFE) units.[12, 19-22] The presence of CFE or CTFE units disrupted the long all-*trans* chain segments due to the high steric hindrance of the Cl atoms yielding a RFE material. The FE nano-domain model was used to explain the observed RFE behavior in these materials, proposing that the introduction of bulky units, such as CFE and CTFE, greatly disrupted local material ordering (as in electron-irradiated P(VDF-TrFE)), producing small FE domains that softened material hysteresis. However, this interpretation was unable to fully explain the appearance of RFE behavior in P(VDF-TrFE) co-polymers with high TrFE content. Liu and co-workers investigated this system and reported on the presence of a morphotropic phase boundary (MPB) around 50% TrFE molar content, where a competition between the all-*trans* and a 3/1 helix conformation takes place.[23-25] Their results showed chain tacticity played a very important role on the polymer FE behavior, and that chain chirality was responsible for the formation of “disordered” helix conformations that lead to RFE behavior.

Accordingly, the study of the polymer structure and chain conformation for these systems is of prime importance in order to decipher their functional behaviors. It has been performed mainly by FT-IR and Raman spectroscopies, and X-ray diffraction techniques. FT-IR studies analyzed the vibration spectra for a variety of PVDF-based polymers, attempting to decipher the origin of the different modes both experimentally and through simulation. It was in these works, prior to the 1980s, that researchers managed to detect and differentiate the three commonly observed phases (α, β, and γ). This was especially difficult given the large number of predicted modes for the γ phase, in many cases overlapping with α and β modes. Raman spectroscopy analysis of these polymers became more frequent between the 1980s and the 2000s, offering an easy, non-invasive, and non-destructive approach to study polymer structure and chain conformation under different conditions (such as temperature, stress, or material polarization). Several works investigated structural changes in PVDF and P(VDF-TrFE) with respect to monomer content and temperature. These studies gave important insight into the evolution of the spectra with increasing TrFE content, showing increases in β phase content with increases in TrFE proportion as well as the appearance of TrFE-unit specific modes.[15, 26-36] Nevertheless, the determination of the polymorphism in PVDF-based polymers has mainly relied on FT-IR spectroscopy combined with X-ray diffraction in the past 20 years. This is particularly true for reports on the FE and RFE properties of PVDF-based ter-polymers. In these systems, it was demonstrated that the introduction of bulky TrFE, CTFE, or CFE units gradually increased the crystalline lamellae interplanar distance, along with the gradual appearance of *tg* defects to the detriment of the all-*trans* conformation. Despite this, the determination of the FE behavior of these materials has relied on an extensive collection of characterization techniques (FT-IR, X-ray diffraction, calorimetry, dielectric spectroscopy, or ferroelectric hysteresis), many of which requiring specific sample preparation that may impact material performance in comparison to real case uses.

Raman spectroscopy offers a facile and non-invasive approach to probe local polymer chain conformation and chain orientation under a wide range of parameters (temperature, excitation wavelength, or wavenumber range), requiring little to no sample preparation. These aspects make it extremely attractive as a quick and easy-to-implement technique to determine polymer functional behavior, with the possibility to integrate into production line quality control at large scale device fabrication.[37] In this work, we utilize Raman spectroscopy to study the evolution in chain conformation of solution-cast P(VDF-TrFE) co-polymers as a function of the TrFE molar content. Raman spectral data are then put into perspective with those from other characterization techniques, including FT-IR spectroscopy, X-ray diffraction (WAXS), calorimetry (DSC), and dielectric spectroscopy (DE), providing a full picture of the underlying chain transformations and consolidating our results. Based on this analysis, we propose a band assignment for the TrFE contributions to the Raman spectra, as well as a defect quantification and chain conformation prediction based on the proposed assignment. These results intend to show the versatility of Raman spectroscopy in the analysis of these ferrotronic materials, potentially predicting their behavior from a straightforward spectral fit and analysis, and expanding this analysis to other PVDF-based co- and ter-polymers.

MATERIALS AND METHODS

Materials. The P(VDF-TrFE) co-polymers used in this study were kindly supplied by Piezotech. According to the manufacturer, the four different co-polymers have a TrFE molar content of 20 %, 25 %, 30 %, and 50 %. Additional information is provided in the Supporting Information (SI). Triethyl phosphate (TEP) was purchased from Sigma-Aldrich.

Polymer Thin Films. Polymer films were made by drop-casting from 15 wt.% solutions in TEP. The solutions were poured onto previously cleaned glass substrates followed by a drying

process of 2 hours 20 min, on a hot plate at 90 °C and atmospheric pressure. Before casting, the solutions were stirred for at least 48h at room temperature. The produced films were detached from the glass substrates through immersion in deionized water, wetting the glass and separating the thin films without deformation or stretching.

Raman Spectroscopy. Raman spectra were recorded with an XploRa spectrometer (Horiba Instruments) coupled with an Olympus microscope, with a linearly polarized laser (Nd:YAG, $\lambda = 532$ nm), at a magnification of 50× (sampling diameter of 10 to 15 μm). No modifications from the laser intensity were observed. The spectra were recorded at ambient conditions after instrument calibration with a Si sample. The spectra were obtained for ranges between 200 and 1600 cm^{-1}. Data treatment included spectral peak detection from 2^{nd} derivative, with derivative 2^{nd} order Savitsky-Golay smoothing; spectral resizing for multiple sample comparison through standard normal variate analysis; and background removal through fitting of 2^{nd} or 4^{th} order polynomials. Peak fitting was performed with Origin and Fityk software using Gaussian and Voigt profiles.

FT-IR Spectroscopy. Spectra were recorded with a Nicolet iS5, with an ATR module iD7 (diamond-crystal window, diameter of 1.8 mm), between 4000 to 400 cm^{-1}. Software in-built ATR spectral correction was used. No sample modifications were observed from the pressure exerted by the sample holder screw. Data analysis was focused on the 1600 to 400 cm^{-1} range, following the same peak detection procedure used in the Raman spectra analysis.

X-ray Diffraction. The crystalline structure was analyzed with a wide-angle X-ray scattering (WAXS) system, Xeuss 2.0 from XENOCS, under vacuum and ambient temperature, with a sample-to-detector distance of 151 mm, and $\lambda = 1.54$ Å (Cu Kα). The diffraction pattern was collecting with a DECTRIS PILATUS-300k detector, for a q range of 0.1 to 3.1 $Å^{-1}$ (1.4° to

46°), followed by azimuthal integration. Data analysis was made with Fityk (software), using Voigt profiles. Additional information on peak fitting is provided in SI.

Calorimetry. Calorimetric analysis was performed with a Differential Scanning Calorimetry (DSC) system (Mettler Toledo DSC 1, with intra-cooler, and N_2 flux). The thermograms were recorded for a maximum temperature range of -50 to 200 °C, at a heating rate of 10 °C min^{-1}. A total of three curves were recorded, corresponding to the first heating, first cooling, and second heating. Only the first heating curves were considered in this analysis, and related to results obtained from the remaining characterization. The melting and Curie transition temperatures were estimated from the minima of the recorded endotherms.

Dielectric Spectroscopy. Broadband dielectric spectroscopy of metal-polymer-metal devices was performed with a Solartron 1260 A impedance analyzer equipped with a Linkam LTS 350 temperature-control system. The measurements were performed with an AC signal of 1 V, at a frequency of 10 Hz, for a maximum temperature range between -60 to 50 °C. The glass transition temperature of the samples was estimated from the loss maximum for the measurements performed at 10 Hz. The device preparation procedure for the dielectric spectroscopy measurements is available in SI.

RESULTS AND DISCUSSION

Films were prepared through solution casting from four different P(VDF-TrFE) with TrFE molar content ranging from 20 to 50 %. All films were dried for 2 h and 20 min at 90 °C under atmospheric pressure. All the used co-polymers present similar molecular weights around 2×10^5 kg mol^{-1} (as determined by SEC – see SI), which we expect to have a negligible influence on property variability between co-polymers when compared to changes induced by TrFE molar content. To decipher the evolution of the chain conformation and crystalline structure as

a function of the TrFE content, Raman and FT-IR spectroscopies were combined with X-ray scattering, calorimetry, and dielectric spectroscopy. This analysis intends primarily to extract valuable information from the Raman spectra, by providing detailed vibration band labelling and relating the changes observed to the structure with respect to the TrFE content. In the literature, the chain conformation analysis has been predominantly made with FT-IR spectroscopy, with only a handful of works providing in-depth discussions of Raman spectra.[15, 26-36, 38-53] Several of these works have performed crystalline band labelling based on theoretical spectral simulations. Simulations of Raman and FT-IR spectra identify the lattice modes of an ideal crystal, calculating the contribution of an infinite crystal lattice. This scenario disregards *tg*-defect formation or the presence of head-to-head chain defects. For this reason, these spectra have shown significant shifts from experimental values (that have been independently reproduced in different works), but have nonetheless aided in the assignment of the experimentally detected bands. In the particular case of P(VDF-TrFE) co-polymers, the nature of the detectable TrFE bands is seldom debated, disregarding potential valuable information on the characterization of the material. Indeed, these changes could then be further related with the polymer structural data, drawing relationships between these different techniques.

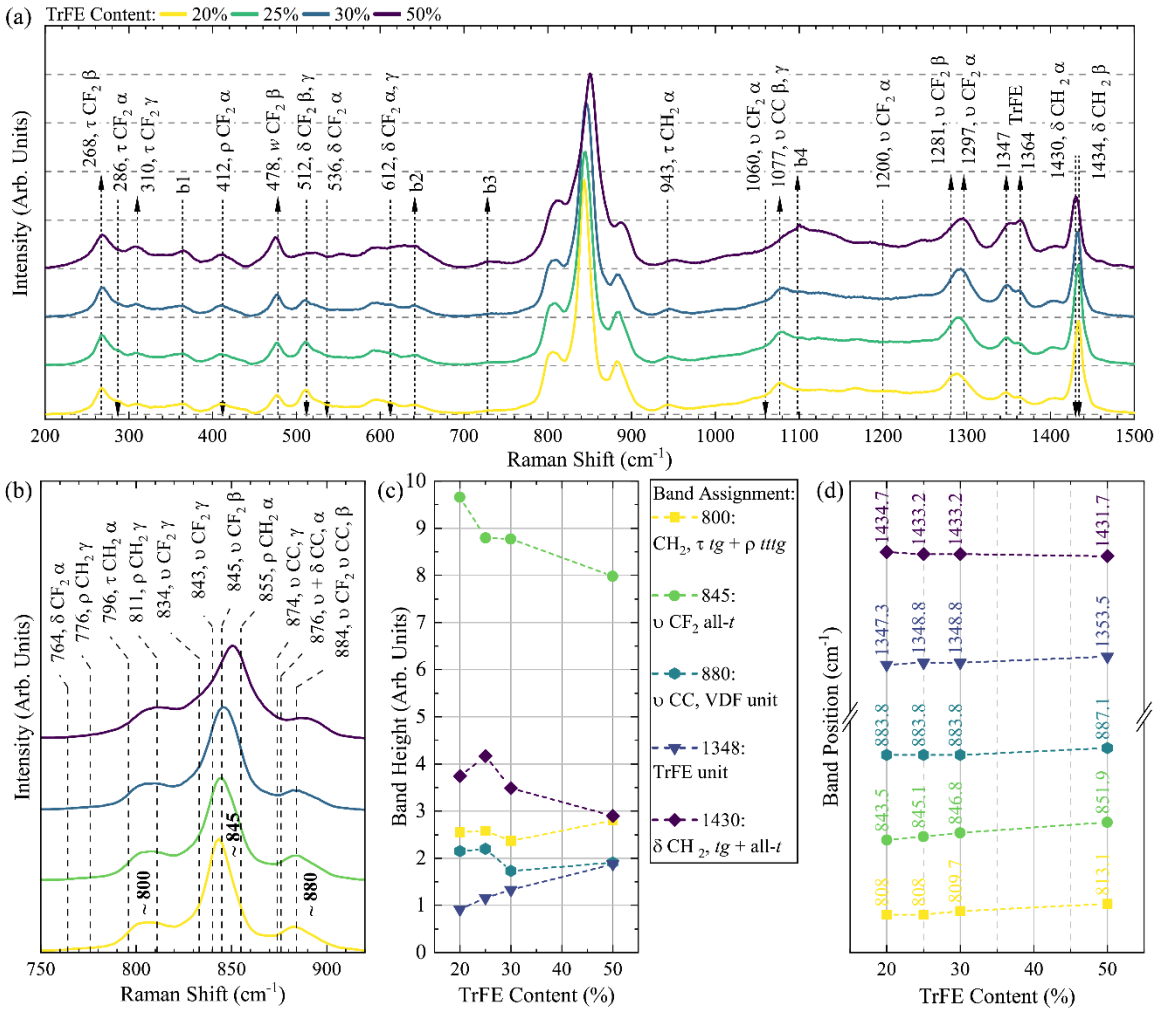

Figure 1. Raman spectra with band assignment, height, and Raman shift (position). a) Raman spectra with band assignment for the different TrFE molar content from 200 to 1500 cm^{-1}. The dashed arrows indicate the direction of increase in band intensity. The bands marked b1 to b4 correspond to bands with no clear assignment. b) Band modes for the range of 750 to 925 cm^{-1}, highlighting the multiple mode contributions to the observed 800, 845, and 880 cm^{-1} bands. c) Raman band height with band assignment for a selection of bands: 800, 845, 880, 1348, and 1430 cm^{-1}. d) Raman band positions as a function of the TrFE content for the same bands as shown in c).

Raman Spectroscopy. The Raman spectra of the different P(VDF-TrFE) films were recorded in the range 200 to 1600 cm^{-1}. This covers most of the modes for PVDF-based polymers. Figure 1 shows the obtained spectra, with the respective band assignment (with type, molecular group, and phases), and extracted band height and position for a selection of crystalline bands. Crystalline band assignment followed several seminal works on Raman and FT-IR

spectroscopy of PVDF homopolymer and P(VDF-TrFE) co-polymers.[36, 38-53] In the literature, bands are typically assigned to specific phases (such as α, β, and γ phases of PVDF), which can lead to misinterpretations. Analysis should focus on the chain conformations associated to the observed modes, in this case, the all-*trans*, *tttg*, and *tg* conformations that are found in the different phases of PVDF-based polymers. Indeed, some bands arising from vibrational modes of *tt*-segments will present overlapping contributions from two distinct phases (in this case, β and γ) and a clear phase attribution cannot be performed. This was addressed by Cai *et al.* as they discussed band assignment and phase determination from FT-IR analysis of PVDF homopolymer through a simple diagram relying on the detection of phase-specific modes.[43] A conformation-oriented analysis can provide important information on chain structure with different parameters.

The Raman spectra shown in Figure 1a can be divided into five regions: 1) 200 and 750 cm^{-1}, 2) 750 and 900 cm^{-1}, 3) 900 up to 1300 cm^{-1}, 4) 1320 and 1380 cm^{-1}, and 5) above 1380 cm^{-1}. The range between 200 and 750 cm^{-1} (zone 1) covers several torsion (τ), wagging (*w*), and rocking (ρ) CF_2 modes, with several CF_2 bending (δ) modes after 500 cm^{-1}. The modes at 268, 478, and 512 cm^{-1} have been associated to all-*trans* segments and constitute a good evidence for the presence of "all-*trans*-phase" in these PVDF-based co-polymers. The band at 512 cm^{-1} often contains an additional contribution at 514 cm^{-1} associated to *tt*-segments in γ-PVDF, and has been observed in several previous works.[41-43, 46] A general increase in all-*trans* specific modes can be seen with increasing TrFE molar content. However, several *tg*-associated modes are still present for all spectra, suggesting the presence of *tg* defects for all TrFE contents. A *tttg* (γ) mode at 310 cm^{-1} is observed to increase with TrFE, though no other phase-specific modes are detected in this range. Additional bands are also present, especially for 50% TrFE, labelled as b1, b2, and b3, which do not correspond to any reported band in PVDF-based

materials. We can speculate that these bands may be associated to *tg*-containing segments, such as *tttg* or $t_{>3}g$, as their intensity increases with TrFE content.

The zone 2 between 750 and 900 cm^{-1} is associated to CH_2 τ and ρ modes (VDF modes), CF_2 stretching (ν) modes, and some CC ν modes (associated to VDF). These bands are typically used in the analysis of PVDF phases in Raman and FT-IR studies. A close-up of this region is shown in Figure 1b. The overlapping modes give rise to three main peaks around 800, 845, and 880 cm^{-1}. The peak around 800 cm^{-1} has contributions from the α and γ, corresponding to *tg* and *tttg*-segments respectively; the 845 cm^{-1} peak contains largely contributions from all-*trans* segments under the form of a CF_2 ν mode, but several early works point to the presence of additional *tttg*-segment modes, around 833 to 843 cm^{-1} (839 cm^{-1} in FT-IR). More recent simulation works showed these *tttg*-modes are expected to have much lower intensity than the all-*trans* specific mode at around 845 cm^{-1}, even for a pure γ sample (for which the band at 811 cm^{-1} appears prominently in the spectra).[44] Lastly, the 880 peak presents multiple VDF-specific contributions from different modes related to different chain segments (at 874, 876, and 884 cm^{-1}). This band is observed to decrease with TrFE content. The most intense peak occurs at around 845 cm^{-1} (ν CF_2) and is associated to β-phase crystallites. As TrFE content increases, the 800 band shifts towards 811 cm^{-1}, which corresponds to a *tttg*-specific mode (ρ CH_2). The main 845 band increases its intensity while also shifting towards higher wavenumbers (increase in all-*trans* segments).

The zone 3 spans from around 900 up to 1300 cm^{-1}, comprising several CC and CF_2 ν modes. This region presents high intensity bands in FT-IR spectroscopy, used to estimate chain defects and phase in several PVDF-based co- and ter-polymers. Despite the weaker response in Raman spectroscopy, a few overlapping bands can still be identified around 1060 to 1070 cm^{-1} (from *tg* and *tt* segments); and around 1280 to 1290 cm^{-1} (all-*trans* and *tg* segments, respectively). The band at 1280 cm^{-1} is a good indication of the presence of β-phase crystallites ($t > 4$) in

PVDF-based materials, often mentioned in FT-IR analysis. Immediately after, zone 4 (1320 to 1380 cm^{-1}) contains modes associated to the TrFE units (around 1347 and 1366 cm^{-1}). This assignment has not always been reported in the literature, with works disregarding these bands, performing wrong mode attribution, or acknowledging its relationship with TrFE without further exploration.[15, 26-36] The neglect is in part due to the low intensity of these bands for low TrFE contents. So far there has not been an exploration of the type of vibration, the associate chain segments, or their relationship with the material behavior or crystallinity, despite reports during the 1980s and 1990s on the synthesis of P(VDF-TrFE) and polytrifluoroethylene (PTrFE) and their IR and Raman spectra.[15, 26-32] An increase in mode intensity is clearly observed with TrFE molar content. Finally, zone 5 comprises the modes above 1380 cm^{-1}, which include several VDF specific CH_2 δ modes. In particular, around 1430 cm^{-1}, three modes can be found at approximately 1427 (not shown), 1430, and 1434 cm^{-1}, corresponding to *tttg*, *tgtg*, and all-*trans* segments. For the considered experimental conditions and TrFE molar compositions, a decrease in these bands is observed with TrFE content.

The variation in band intensity and band position is plotted in Figure 1c-d, for the bands located at *ca.* 800, 845, 880, 1348, and 1430 cm^{-1}, corresponding to: the 796 + 811 cm^{-1} group (*tg* τ and *tttg* ρ, CH_2); the 843 + 845 cm^{-1} group (*tttg* + all-*trans*, CF_2 ν); the CC ν modes (VDF, all conformations); one of the observed TrFE unit modes; and the 1430 + 1434 cm^{-1} group (*tg* and all-*trans*, CH_2 δ), respectively. Several observations can be made from such a representation. Firstly, the 845 cm^{-1} band is most intense for a TrFE content of 20 %, after which it gradually weakens, consistent with previous reports on the favorable formation of β-phase crystalline domains in P(VDF-TrFE).[54, 55] Secondly, the 800 cm^{-1} band increases (especially for 50 % TrFE), pointing to an increase in *tg* or *tttg* conformations in VDF-segments and agreeing with other low intensity *tg* and *tttg* modes (*tttg* specific mode at 310 cm^{-1}) observed in the spectra. Lastly, the VDF-specific 880 cm^{-1} band shows a decrease with TrFE, in accordance with the

gradual replacement of the VDF units by TrFE. It is interesting to note that the TrFE band at 1348 cm^{-1} increases in intensity, but not linearly. The opposite is observed with the VDF band at 1430 cm^{-1}, which decreases with the TrFE content.

The shifts in band position, shown in Figure 1d, also proved instructive. These shifts are most significant in the case of the 800 cm^{-1} band, which rises from 808 to 813 cm^{-1} (consistent with an increase in *tttg* segments); and the 845 cm^{-1} band, which initially lies at 843 cm^{-1} and shifts to around 852 cm^{-1}. The observed band position shifts (towards higher energy) can be associated to stress, changing the molecular environment. This behavior will be further discussed in the next sections (*vide infra*). Finally, the 1430 cm^{-1} band initially appears around 1434 cm^{-1}, shifting towards 1431 cm^{-1}. As no α-specific modes are clearly observed for a TrFE content of 50%, we can assert that this shift towards 1430 cm^{-1} is due to the observed decrease in band intensity combined to the slow increase in *tttg* modes (in this case, a small overshadowed contribution from the band at 1427 cm^{-1} that shifts the convoluted peak towards low wavenumbers).

In summary, the prepared samples are primarily composed of long all-*trans* segments, and should be expected to present high β-phase content (thus a more ferroelectric behavior). Nevertheless, the gradual appearance of defects with TrFE content is clear (especially *tttg*-segments) marked by band position shifts, the persistence of low intensity bands from *tg*-segments (but the absence of α-specific modes), and the appearance of the 310 cm^{-1} band (*tttg*-specific).

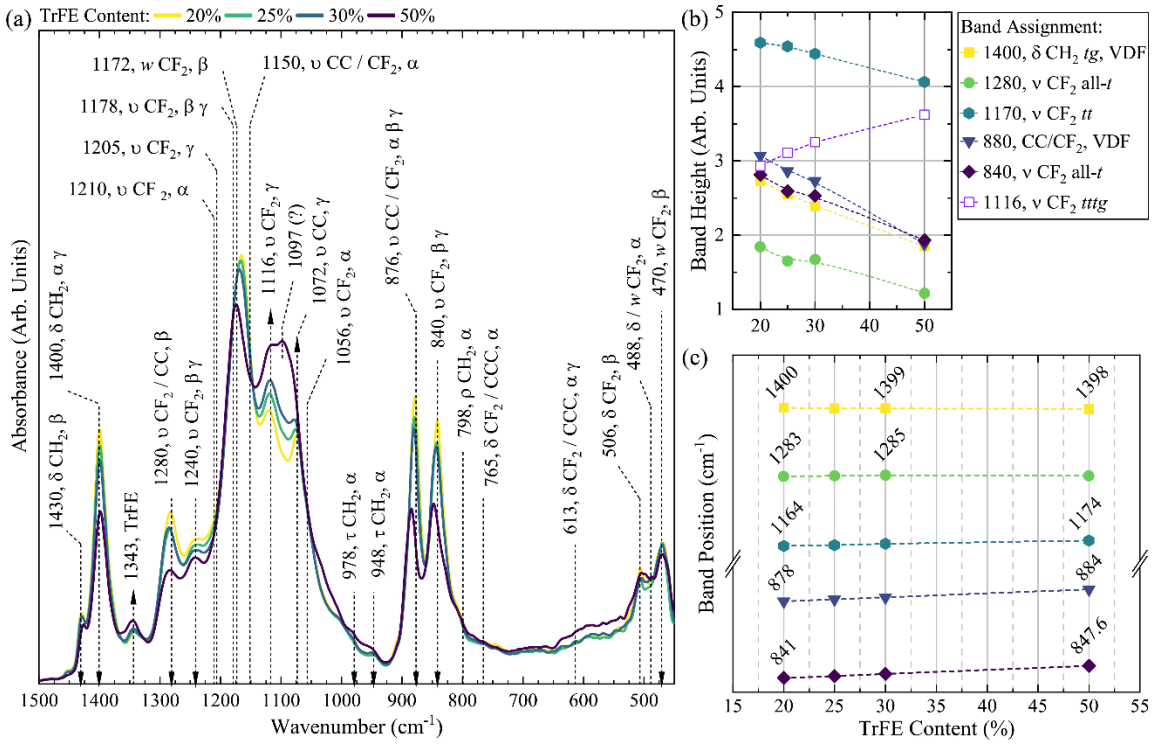

Figure 2. FT-IR spectra, and band height and shift as a function of TrFE content. a) FT-IR spectra for samples with different TrFE molar content, with respective band labeling and phase assignment. Multiple phases can be associated to the same band. b) Band height for a selection of β-specific (840, 1170, and 1280 cm^{-1}), γ (1116 cm^{-1}), and VDF modes (880 and 1400 cm^{-1}) with TrFE content. c) Band shifts for the same bands shown in b).

FT-IR Spectroscopy. Complementary FT-IR characterization was performed in order to relate the experimental observations between the two techniques. The FT-IR spectra are plotted in Figure 2a, with the assignation of several bands to their associated phases and type of vibration. Several β-specific modes are present for all compositions (470, 506, 840, 1172, 1280, and 1430 cm^{-1}). The range 900-1300 cm^{-1} (zone 3 in Raman) is particularly more active in FT-IR and provides additional information. A gradual increase in a γ-related mode is observed around 1116 cm^{-1} (arising from *tttg*-segments), as well as other shared modes from *tt* and *tg* segments. An additional band can also be seen around 1097 cm^{-1} (marked with "?"), the origin of which is unclear, as previous works have not reported the presence of any band at this location. Considering its location, it is likely that this mode arises from *tttg* or *tg* segments, as a gradual increase in these modes is observed with increasing TrFE content. The same band was also

detected in the Raman spectra, labelled as b4 (see Figure 1a), albeit with a much lower intensity. The 1343 cm^{-1} TrFE band is also visible, although it increases only slightly with the TrFE molar content. The 1364 cm^{-1} TrFE band is overshadowed by the 1400 cm^{-1} band, which is more active in FT-IR. This shows that Raman spectroscopy is a more suitable technique to analyze changes in this spectral region linked to the TrFE bands. Peak height and position are plotted in Figure 2b and 2c. The same tendencies as those retrieved in Raman spectroscopy are also observed, with maxima in β-specific modes (840, 1170, and 1280 cm^{-1}) occurring for TrFE contents of 20 %. The VDF-specific 880, 1400, and 1430 cm^{-1} (the latter less active in FT-IR) decrease with TrFE, in line with the Raman spectra. Several band shifts are detected, with β-specific modes shifting towards high wavenumbers. The 1400 cm^{-1} band presents a shift towards low energy (as the 1430 cm^{-1} bands in Raman). The presence of these two bands in Raman and FT-IR (with different activity) and arising from different conformations of the VDF units demonstrate that despite the high content of β-phase, there are still several VDF chain segments presenting *tttg* and *tg* conformations in-between long all-*trans* segments. These *tg*-defects may arise from within the crystalline domains but also from the crystalline-to-amorphous boundaries where a certain degree of long range ordering may still exist (oriented amorphous fractions).[56, 57] The FT-IR spectra agrees very well with the tendencies observed from the Raman spectra. In particular, FT-IR analysis confirmed the increase of defective conformations with TrFE molar content (such as *tttg* and *tg* segments), such as the case of the bands at 1072 and 1116 cm^{-1}.

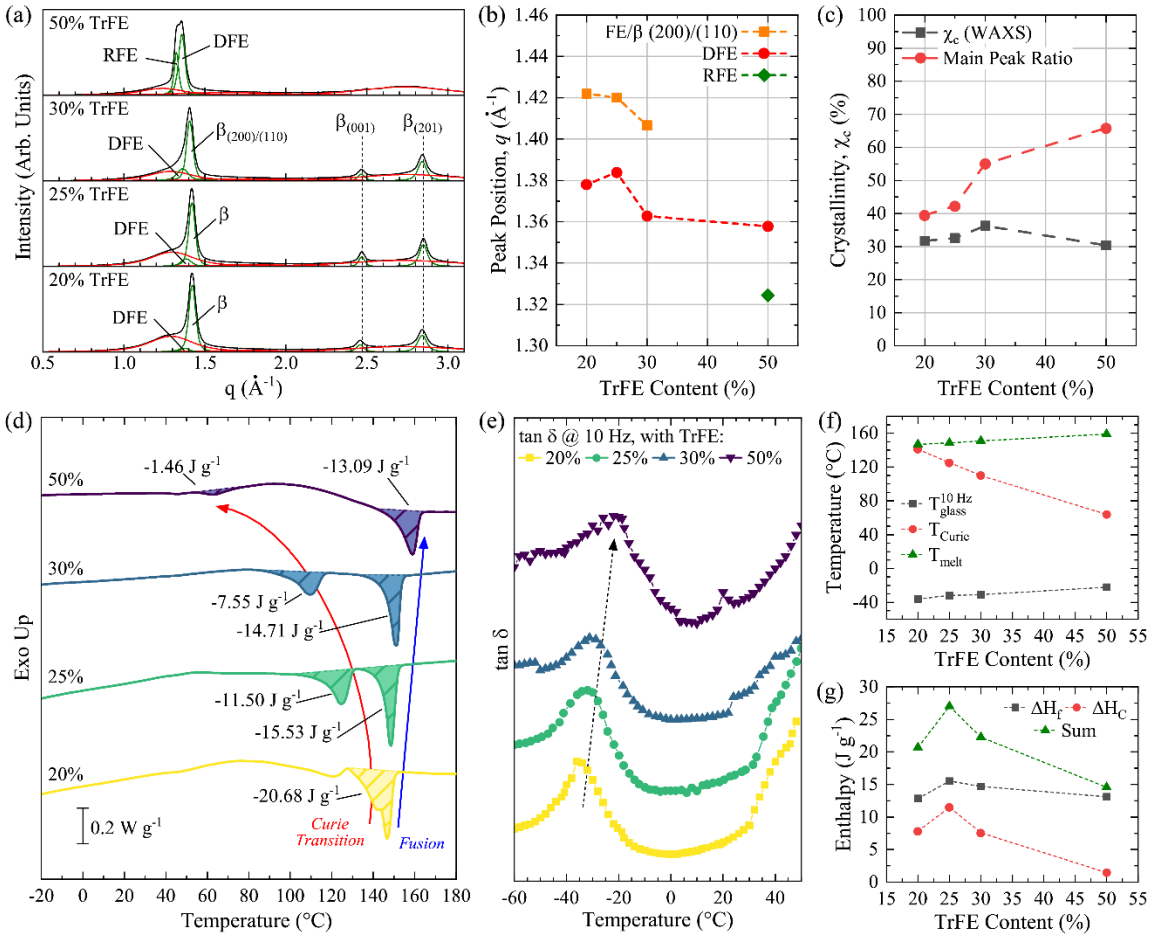

Figure 3. X-ray diffraction patterns, calorimetry, and dielectric spectroscopy. a) Diffraction patterns for the considered samples, with peak labelling. b) Peak position, in q, extracted from the pattern fitting functions in a). c) Crystallinity and main peak ratio calculated from the crystalline peak area. d) DSC thermograms, showing the shift in melting temperature (blue arrow) and Curie transition temperature (red arrow). The areas of the endotherms are also shown. e) Permittivity loss factor, tan δ, at 10 Hz, as a function of temperature, showing a shift of the glass transition temperature (dashed black arrow) towards higher temperatures. f) Plot of the transition temperatures ($T_{glass}^{10\ Hz}$, T_{Curie}, and T_{melt}) estimated from the DSC and DE data shown in d) and e), respectively. g) Plot of the fusion enthalpy (solid-liquid, ΔH_f), Curie transition enthalpy (solid-solid, ΔH_C), and their sum, obtained from endotherm integration from d). The values for 20% TrFE were extrapolated from an endotherm deconvolution (see SI, Figure 2S).

X-ray Structural Analysis. The structure of the P(VDF-TrFE) films was assessed with wide-angle X-ray scattering (WAXS). The azimuthally integrated diffraction patterns and the respective fittings (see SI for additional information) are shown in Figure 3a. Several diffraction peaks were identified for all compositions: the ferroelectric (FE) β phase with

pseudo-hexagonal/orthorhombic unit cell (20 to 30 % TrFE); the defective ferroelectric (DFE) phase (all co-polymers); and the relaxor-ferroelectric (RFE) phase for 50 % TrFE. For the 20 to 30 % TrFE, the main detected phase corresponded to the FE β phase, with the most intense reflection associated to the (200)/(110) peak around 1.42 $Å^{-1}$. It was already reported that DFE phases can arise in PVDF co- and ter-polymers with TrFE and low amounts of CFE or CTFE due to the increase in the interplanar distance and the incorporation of *tg* defects along the polymer chain, disrupting long-range ferroelectric ordering.[58, 59] The increase in chain defect occurrence (from the increase of TrFE, CFE, or CTFE) has been linked to the eventual transformation of this DFE phase into a relaxor-ferroelectric (RFE) phase.[58] This is the case for the sample with 50 % TrFE content, which presents two diffraction peaks associated to a RFE and a DFE phase (at 1.32 and 1.36 $Å^{-1}$, respectively), with the disappearance of the FE β phase. The presence of a RFE phase for 50% TrFE is consistent with previous reports on the presence of a morphotropic phase boundary around this TrFE proportion, leading to a competition between FE/DFE and RFE phases, after which the RFE becomes the dominant phase.[23-25, 60] In addition, no crystalline bands were detected in Raman or FT-IR that correspond to a PE phase (α-specific, *tgtg'*), which further corroborates that the detected diffraction peaks correspond to a RFE and DFE phases. The extracted peak positions (in *q*) from the fitted data are plotted in Figure 3b for the FE, DFE, and RFE. The positions decrease in *q* (*i.e.*, an increase in the interplanar distance) due to the incorporation of TrFE units inside the crystalline lamellae. The potential incorporation of *tg* defects inside the crystalline lamellae is also expected to play an important role in the increase of the interplanar distance for high TrFE contents, as backed up by the Raman and FT-IR spectra. The absence of crystalline diffraction peaks at high *q* (above 2.4 $Å^{-1}$) for a 50 % TrFE content suggests a significant disruption in long range chain ordering. The diffraction planes associated to these reflections [(001) and (201)] contain a *c*-axis component (chain axis), and their absence may point to a disruption on

chain ordering from the appearance of *tg* segments. This observation is consistent with recent interpretations on the origin of relaxor behavior in the PVDF family of co- and ter-polymers.[23-25] These works highlight the formation of a disordered 3/1 helix structure due to the chirality of the TrFE (or CTFE) monomer, disrupting structural and ferroelectric long-range ordering.

The crystallinity (χ_c) was estimated from the diffraction patterns (ratio of crystalline peak area to total pattern area). The values are plotted in Figure 3c, with χ_c increasing up to 38 % for a 30 % TrFE content, decreasing to around 30 % for 50 % TrFE. A recent work by María *et al.* reported on the crystallization kinetics of molten bulk P(VDF-TrFE) co-polymers, showing that the inclusion of TrFE inside the PVDF-crystals increased nucleation rate and density.[61] This work deals with solution cast and dried thin films, in which solvent-polymer interaction is expected to have an important contribution. In the considered conditions, high TrFE content appears to promote higher crystallinity. The observed decrease for a TrFE content of 50 % could be explained by the absence of high *q* diffraction peaks, reducing χ_c. This may not entail a decrease in sample crystallinity, but rather a disruption in chain long-range ordering (particularly along the *c*-axis). In fact, if we calculate the main peak ratio considering only the contributions between 1.0 to 1.6 $Å^{-1}$ (also shown in Figure 3c), we observe that it increases constantly with the TrFE content due to the decrease of the amorphous halo around 1.2 to 1.3 $Å^{-1}$.

Calorimetry and Dielectric Spectroscopy. Calorimetry is often used to estimate χ_c in these polymer systems. However, the variation of the enthalpy of fusion (ΔH_f^0) with TrFE in P(VDF-TrFE) is not established, with several works utilizing reported values with variations of 5 to 10 % from the experimentally used proportions. ΔH_f^0 of 93 and 67 J g^{-1} have been reported for PVDF and PTrFE homopolymers, respectively, with more recent works reporting values

around 40 J g^{-1} for P(VDF-TrFE) with 20 % TrFE.[62-65] These values show ΔH_f^0 in P(VDF-TrFE) co-polymer systems has a non-linear response, and an extrapolation is not sufficient to properly estimate χ_c for a large array of molar fractions.

Nonetheless, calorimetry provides important information on transition temperatures. DSC was performed and the resulting endotherms plotted in Figure 3d, for the first heating scan. The melting (solid-liquid transition, T_{melt}) and Curie (solid-solid transition, T_{Curie}) transition temperatures present opposite tendencies, with the T_{melt} increasing with the TrFE content (blue arrow), while T_{Curie} decreases (red arrow). At 20 % TrFE, T_{Curie} approaches T_{melt} resulting in two overlapping endotherms. The T_{Curie} shift towards low temperature is in line with the observed phases from the X-ray diffraction data, with the increase in TrFE resulting in a loss of dipolar long-range coherence (especially for high TrFE contents). The permittivity loss factor (shown in Figure 3e), tan δ, as a function of temperature (at 10 Hz) was recorded with dielectric spectroscopy (DE) allowing the estimation of the glass transition temperatures ($T_{glass}^{10\ Hz}$). The maxima around -40 °C correspond to $T_{glass}^{10\ Hz}$, shifting to higher temperatures with TrFE content. The estimated transition temperatures from DSC and DE ($T_{glass}^{10\ Hz}$, T_{Curie} and T_{melt}) are plotted in Figure 3f, showing approximately linear tendencies with TrFE, for the considered proportions. The increase in T_{melt} with TrFE content is consistent with previous early works on P(VDF-TrFE) co-polymers that analyzed transition temperatures in this system. The T_{Curie} decrease is also in agreement with the literature, stabilizing at lower temperatures for high TrFE content. This decrease signifies a shift towards a RFE phase.[63, 66]

The enthalpies of fusion and Curie transition (ΔH_f and ΔH_C, respectively) are plotted in Figure 3g, along with their sum. The values for 20 % TrFE were extrapolated from the deconvolution of the endotherm by fitting with two Pearson IV functions (see SI, Figure S2). The highest values of ΔH_C are obtained for 25 % TrFE. This would suggest the largest amount of

electroactive phases is found for 25 % TrFE despite the fact that this TrFE proportion presents a lower T_{Curie}, a similar χ_c, and less intense all-*trans* modes maxima (Raman and FT-IR) when compared to 20 % TrFE. Another possibility to explain this discrepancy may be related to the solid-solid phase transition enthalpy, which for 25 % TrFE may be higher than for 20 %. As far as the authors know, no systematic study has been performed on potential variations on solid-solid phase transition enthalpy on these co-polymer systems. ΔH_f follows a distinct trend, presenting the lowest values for 20 % TrFE (12.8 J g^{-1}, extracted from fitting), followed by 50 % TrFE (at 13.09 J g^{-1}), and retaining values around 15 J g^{-1} for the remaining TrFE proportions.

Deciphering the Effects of TrFE on Raman Spectra. Following the additional analysis with WAXS, DSC, and DE, we can now address the band broadening and shifting observed in the Raman (and FT-IR) spectra. Signal broadening is associated to loss in vibration coherence, while band shifts are associated to vibration energy shifts induced by changes in molecular interactions or bond compressive/tensile stresses. In the spectra in Figure 1a-b, we can see a gradual broadening of the 845 cm^{-1} band, corresponding to an all-*trans* CF_2 ν mode. We can quantify the degree of broadening by performing a non-linear multi-peak fitting (see SI for details) for the bands located in this range (*ca.* 750 to 920 cm^{-1}) and extracting the height and breadth of the 845 cm^{-1} band. As material crystallinity and the relative amount of all-*trans* segments directly impact the intensity of this band, we can attempt to remove these contributions by calculating the ratio between peak FWHM and height. This ratio is plotted in Figure 4a, where it shows a minimum for 20 % TrFE, after which it increases steadily. The curve suggests that this vibration mode presents high coherence for 20 % TrFE (*i.e.*, the highest all-*trans* content). The vibration coherence then decreases as the TrFE molar content increases. The all-*trans* CF_2 ν mode is of particular importance given the direction of the vibration with

443 respect to the chain backbone, *i.e.*, having a perpendicular projection to the chain, as illustrated
444 in Figure 4a. This component is also parallel to the monomer dipolar moment (μ, which is
445 perpendicular to the polymer backbone, or *c*-axis), and may serve as an indicator for dipolar
446 long-range ordering. This is consistent with the variation of the T_{Curie} extracted from the DSC
447 data (Figure 3d and 3f). The highest T_{Curie} was obtained for 20 % TrFE, entailing long-range
448 dipolar ordering, after which it decreases due to a decrease in dipolar ordering from the increase
449 in inter-chain spacing (as attested by the X-ray data). It is also important to mention that phonon
450 confinement effects can also play an important role on the observed band broadening.[67] This
451 confinement effect originates from the gradual formation of *tg*-defects along all-*trans*
452 segments, producing an asymmetrical band broadening. However, the complex band
453 contribution in this region hinders the proper detection of a biased broadening effect.

454 The band shifts can be analyzed considering the effects of the TrFE units and defect
455 incorporation into the polymer structure. Considering the diffraction peaks at high *q* values
456 (see Figure 3a), we can express the relative spacing variation with respect to the peak positions
457 for 20 % TrFE. This is plotted in Figure 4b, for the diffraction peaks associated to the (001),
458 (201), and (110)/(200) planes. The (001) and (201) planes containing the *a* and *c*-axis of the
459 unit cell present negligible relative variations, lower than 1 %; while the (110)/(200) plane
460 increases its relative spacing, reaching almost 5 % for the DFE-phase at 50 % TrFE. As the
461 (201) plane includes an *a*-axis component and presents minor variations, we can conclude that
462 the unit cell expands non-uniformly in the *b*-axis, experiencing compressive stress along the *a*
463 and *c*-axis as more TrFE units are incorporated into the polymer chain. This anisotropic unit
464 cell expansion is likely responsible for the band shift observed in both Raman and FT-IR
465 spectroscopy.

466

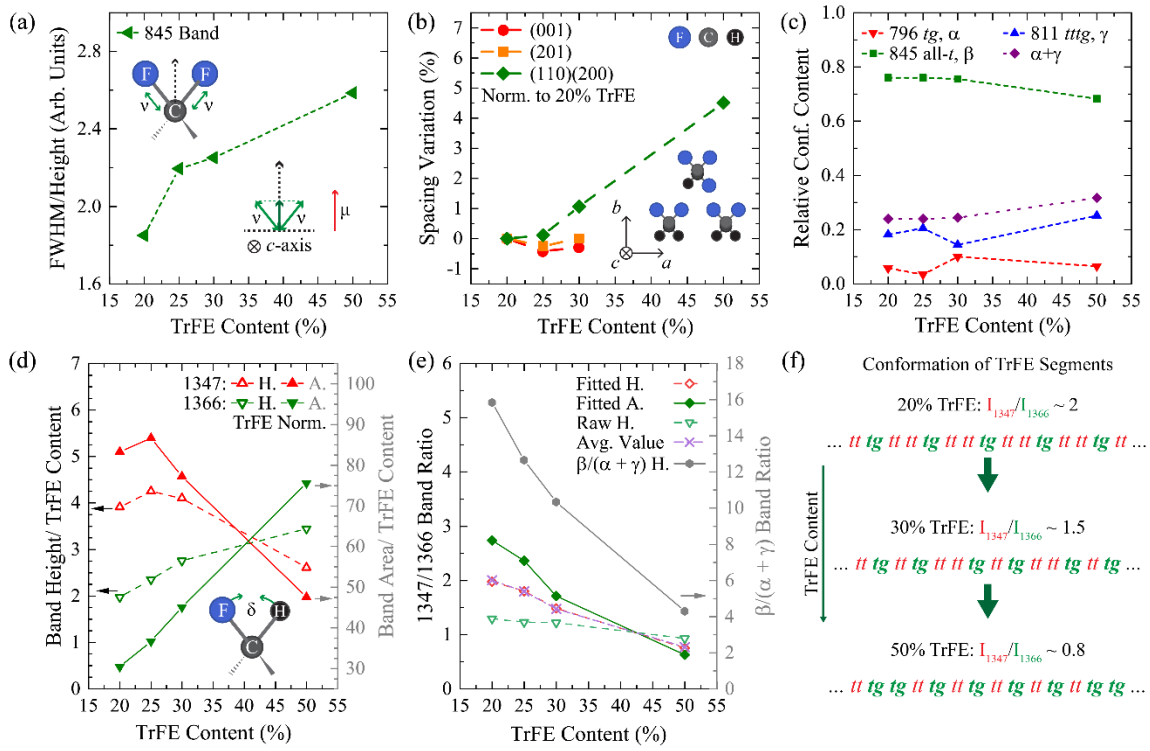

Figure 4. Band broadening, shifting, and ratios from X-ray and Raman data. a) 845 cm^{-1} all-*trans* CF_2 ν mode band broadening normalized to peak height *vs.* TrFE content, with illustration of the vibration geometry relative to the chain *c*-axis and dipolar moment, μ. b) Relative unit cell diffraction plane spacing variation (with respect to 20 % TrFE) for the (001), (201), and (110)/(200) diffraction planes as a function of the TrFE content. An illustration of the all-*trans* orthorhombic unit cell is also shown, seen from the direction of the *c*-axis. c) Relative conformation content *vs.* TrFE molar content, calculated from the height of the 796, 811, and 845 cm^{-1} fitted Raman bands. d) Evolution of the band height and area of the 1347 and 1366 cm^{-1} TrFE bands, extracted from spectral fitting, and normalized to the TrFE content. An illustration of the vibration mode is also shown. e) Band height and band area ratios for the 1347 cm^{-1} *tt* and 1366 cm^{-1} *tg* TrFE bands, extracted from the fitted data (Fitted H. and Fitted A.) and the raw data (denoted as Raw H.), and the calculated average value (Avg. Value) from all the data sets. The calculated average coincides with the fitted band height values. The β (all-*trans*) to α+γ (*tg* + *tttg*) band height ratios (in gray, left axis) are also plotted, extracted from the same fitted data utilized in c). f) Illustration of the chain conformation within the TrFE segments, with decrease of the number of *tt*-segments between each *tg*-segment with increases in TrFE content. The ratios I_{1347}/I_{1366} represent the band intensity [height or area, plotted in e)] ratios between the bands 1347 and 1366 cm^{-1}.

TrFE-specific Raman Bands and Defect Quantification. The different characterization techniques reveal important information on the evolution of the chain conformation with TrFE content. We start by addressing the origin of the TrFE vibration bands, especially clear in

Raman spectroscopy. The inverse relationship between the 1347 and 1430 cm^{-1} bands (Figure 1a and 1c) is a good indication of their nature. Based on well-established spectroscopic data of high polymers[28, 68] combined with the observed behavior in the recorded spectra, we are able to infer the mechanism behind the evolution of the 1347 and 1366 cm^{-1} TrFE bands. It is well-known that the CH_2 deformation in PVDF is shifted towards low wavenumbers in comparison to polyalkenes, such as polyethylene or polypropylene, due to the presence of the F atoms that reduce the vibration frequency of the δ CH_2 modes.[68] The addition of another F atom, as is the case of the TrFE unit, should further shift the vibration frequency of this mode towards lower energies, having a vibration dampening effect. Considering the decrease in the 1430 cm^{-1} δ CH_2 mode, we can associate the 1347 and 1366 cm^{-1} bands as arising from CHF deformation modes (δ CHF) in the TrFE units.

On the basis of this hypothesis, we can further explore the chain conformation related to these two bands by gathering evidence from the characterizations carried out. Firstly, we can use the data obtained from the 845 cm^{-1} band fitting (as discussed above; see SI, Figure S3) to infer the overall relative conformation content based on the intensity of the fitted peaks for the 796, 811 and 845 cm^{-1} bands. This is plotted in Figure 4c, with the highest relative all-*trans* content obtained for TrFE contents of 20 % up to 30 %. An increase in the *tttg* conformation is then seen for 50 % TrFE, in line with the appearance of other *tttg* related bands in other zones of the Raman and FT-IR spectra. This is also validated by the presence of the RFE phase in the X-ray diffraction pattern, as well as the decrease in the magnitude of T_{Curie} and ΔH_C in the DSC data. We can apply the same analysis to the two TrFE bands at 1347 and 1366 cm^{-1} and perform a multi-peak fitting with several Gaussian and Voigt profiles between the range of 1270 and 1500 cm^{-1} (see SI, Figure S4), extracting the height and the area of these bands. As the intensity is also proportional to the amount of TrFE, we should normalize the extracted data by the TrFE molar content. The normalized peak height and area for the two bands is plotted in Figure 4d

for the considered TrFE molar contents. These two bands present approximately mirrored behaviors with similar tendencies as those observed in Figure 4c. This suggests that these two bands arise from different chain conformations, and a clear shift is detected with the variation of the TrFE molar content. Considering these observations and the overall increase in *tg* chain defects supported by the different characterization techniques, we propose that the two TrFE bands at 1347 and 1366 cm^{-1} are associated to δ CHF modes arising from two different chain conformations, namely, a *tt* and *tg* conformation, respectively.

This band assignment opens the possibility for defect quantification in P(VDF-TrFE) co-polymers by measuring and fitting these two bands from Raman spectroscopy data. In particular, it offers a way to quantify TrFE *tg* defect occurrence along the polymer chain by focusing on the height or area ratio of the 1347 and 1366 cm^{-1} bands. This is shown in Figure 4e, where the 1347 and 1366 band height and area ratios are plotted from the fitted (Fitted H. and Fitted A.) and raw data (Raw H.), along with the ratio average value (Avg. Value). The β/(α+γ) [alternatively, *tttt*/(*tg* + *tttg*)] band height ratio is also shown, obtained from the fitted data (796, 811, and 845 cm^{-1}) used in the calculation of the relative conformation content (Figure 4c). All the plotted data present the same tendencies with increasing TrFE content, indicating an increase in the amount of *tg* defects along the polymer chain. The β/(α+γ) ratio presents values above the 1347/1366 ratio, suggesting the VDF segments present higher amounts of all-*trans* sequences in relation to *tg* sequences. It is very important to note that the bands at 796 and 811 cm^{-1}, commonly used to estimate phase proportion in PVDF-based co-polymers, arise from VDF-specific segments corresponding to CH_2 vibration modes. Our relative conformation estimation does not account for the mode intensity loss from the reduction in VDF segments with TrFE content, meaning the β/(α+γ) ratio may be overestimated, and the VDF units may present a higher defect content than previously suggested. This is also an aspect that has not been addressed in previous works, many of which

have relied on band intensity to estimate phase proportion in different processing and composition studies. Interestingly, the 1347/1366 ratio also suggests that TrFE containing chain segments already present *tg* defects even for low TrFE content. These *tg* defects may be incorporated into the polymer crystallites and be responsible for the increase in unit cell volume along with the incorporation of TrFE units, resulting in the observed DFE phases. The larger value discrepancy between the ratios calculated from fitted height and area for low TrFE contents can be explained by the error associated with multi-peak fitting for low intensity bands that are easily overshadowed by other more intense contributions.

Recent literature has highlighted the importance of *tg* defects along the polymer chain, being responsible for the appearance of RFE behavior.[23-25] In 2020, Liu *et al.* reported on this effect, and demonstrated how the chiral nature of the TrFE monomer leads to the formation of a disordered 3/1 helix chain, with a $(tg)_3$ conformation.[24] Following the results discussed in this article, we should expect to observe an intense vibration band around 1366 cm^{-1} for a 3/1 helix structure with $(tg)_3$, corresponding to the *tg* δ CHF, with a very small to negligible contribution at 1347 cm^{-1}. This trend is indeed observed with the gradual increase of TrFE reducing the contribution of the 1347 in favor of 1366 cm^{-1}, pointing to an increase in *tg* defects within the TrFE segments. The ratio of these two bands may constitute a probe into the conformation of the TrFE segments, with ratios above 1 and below 1 signifying a majority of *tt*-segments or a dominance by *tg*-segments, respectively. We can note from Figure 4e, that the 1347/1366 ratio drops continuously, from around 2 to a value around 0.8 for 50 % TrFE. An illustration of the chain structure based on the 1347/1366 ratio (I_{1347}/I_{1366}) is depicted in Figure 4f, where the chain conformation is represented for different contents of TrFE. The gradual increase of TrFE decreases the length of the all-*trans* segments, with the ratio I_{1347}/I_{1366} representing the approximate total number of *tt*-segments periodically separated by *tg* defects within the TrFE segments of the polymer chain. A RFE phase is detected in this work for 50 % TrFE, for which

$I_{1347}/I_{1366} < 1$, *i.e.*, a *tg*-dominated chain structure that gradually approaches the 3/1 helix structure. From the extrapolation of the calculated data, it can be seen that $I_{1347}/I_{1366} < 1$ occurs around 45 % TrFE, the same proportion where the 1347 and 1366 bands height (area) inversion takes place (Figure 4d). This proportion has previously been linked to the start of the morphotropic phase boundary (around 45 % to 55 % TrFE) in P(VDF-TrFE) co-polymers. As a result, a quantitative relationship has been established between specific band ratios and the occurrence of *tg* defect in PVDF-based polymers, in good agreement with recent literature on the structure and FE behavior of P(VDF-TrFE) co-polymers.[23-25]

CONCLUSION

In this work, we have analyzed the Raman spectra of P(VDF-TrFE) co-polymers for various TrFE proportions. Under the considered conditions (solution-cast, no thermal annealing), the co-polymers presented β phase (all-*trans*) specific vibration modes, with an increase in defective modes (*tg* and *tttg* containing modes) for higher TrFE molar content. TrFE-specific modes, whose intensity increases with TrFE content, were detected at 1347 and 1366 cm^{-1}, and show opposite evolution to the surrounding VDF modes at 1430 cm^{-1}. Complementary FT-IR analysis confirms these observations, with the highest intensity of all-*trans* modes found for 20 % TrFE, and with several *tttg*-specific modes appearing for higher TrFE contents (at 1056 and 1116 cm^{-1}). X-ray diffraction showed that the majority phase corresponded to the FE β phase, with traces of a minor DFE phase. For 50 % TrFE, a RFE phase was observed with DFE as the majority phase. Material crystallinity for the solution-cast films increased with TrFE content, but was observed to decrease for 50 % TrFE, suggesting enhanced nucleation for proportions around 30 %. DSC and DE showed an increase in the melting and glass temperatures (T_{melt} and $T_{glass}^{10\,Hz}$) and a decrease of the Curie transition temperature (T_{Curie}).

589 Following these results, we have proposed that the two detected TrFE bands at 1347 and 1366
590 cm^{-1} are associated to δ CHF modes arising from a *tt* and *tg* conformation, respectively.
591 Monitoring of the 1347/1366 intensity ratio (I_{1347}/I_{1366}) was proposed as a potential probe into
592 the structure of the TrFE-segments: ratios above 1 represent a majority of *tt*-segments, while
593 ratios below 1 represent a dominance by *tg*-segments. The extrapolated inversion in the 1347
594 and 1366 cm^{-1} bands intensity also takes place for TrFE molar fractions corresponding to the
595 reported morphotropic phase boundary for P(VDF-TrFE). Accordingly, a quantitative
596 relationship has been drawn for the first time between specific band ratios and *tg* defect
597 occurrence in PVDF-based polymers. We expect this method to also be applicable to other
598 PVDF co- and ter-polymers containing chiral monomers (like CTFE or CFE).

599

600 ASSOCIATED CONTENT

601 **Supporting Information**

602 The Supporting Information is available free of charge at.

603 Additional information on polymer molecular weight from SEC. Polymer thin film
604 fabrication for dielectric spectroscopy. Multi-peak non-linear fitting of the X-ray diffraction
605 patterns. Multi-peak non-linear fitting of the DSC endotherm for 20% TrFE. Multi-peak non-
606 linear fitting of the Raman spectra.

607 AUTHOR INFORMATION

608 **Corresponding Author**

609 **Pedro M. Resende** - Université de Bordeaux, CNRS, Bordeaux INP, LCPO, UMR 5629, F-
610 33600, Pessac, France. ORCiD: orcid.org/0000-0001-7854-2297. Email: pdecamposres@u-
611 bordeaux.fr

Authors

Jean-David Isasa - Université de Bordeaux, CNRS, Bordeaux INP, LCPO, UMR 5629, F-33600, Pessac, France.

Georges Hadziioannou - Université de Bordeaux, CNRS, Bordeaux INP, LCPO, UMR 5629, F-33600, Pessac, France. ORCiD: orcid.org/0000-0002-7377-6040

Guillaume Fleury - Université de Bordeaux, CNRS, Bordeaux INP, LCPO, UMR 5629, F-33600, Pessac, France. ORCiD: orcid.org/0000-0003-0779-191X

Notes

The authors declare no conflicts of interest.

ACKNOWLEDGEMENTS

The authors acknowledge the financial support from the Industrial Chair SMILE within the Grant Agreement No. ANR-19-CHIN-0002. The authors thank Arkema-Piezotech (France) for providing the materials used in the study. P.M.R. would like to thank Sara Zanchi for insightful discussions.

REFERENCES

1. Valant, M., Electrocaloric materials for future solid-state refrigeration technologies. *Progress in Materials Science* **2012,** *57* (6), 980-1009.
2. Ožbolt, M.; Kitanovski, A.; Tušek, J.; Poredoš, A., Electrocaloric refrigeration: Thermodynamics, state of the art and future perspectives. *International Journal of Refrigeration* **2014,** *40*, 174-188.
3. Li, Q.; Wang, Q., Ferroelectric Polymers and Their Energy-Related Applications. *Macromolecular Chemistry and Physics* **2016,** *217* (11), 1228-1244.
4. Prateek; Thakur, V. K.; Gupta, R. K., Recent Progress on Ferroelectric Polymer-Based Nanocomposites for High Energy Density Capacitors: Synthesis, Dielectric Properties, and Future Aspects. *Chemical Reviews* **2016,** *116* (7), 4260-4317.

5. Chen, X.; Han, X.; Shen, Q.-D., PVDF-Based Ferroelectric Polymers in Modern Flexible Electronics. *Advanced Electronic Materials* **2017,** *3* (5), 1600460.
6. Fähler, S., Caloric Effects in Ferroic Materials: New Concepts for Cooling. *Energy Technology* **2018,** *6* (8), 1394-1396.
7. Li, H.; Liu, F.; Fan, B.; Ai, D.; Peng, Z.; Wang, Q., Nanostructured Ferroelectric-Polymer Composites for Capacitive Energy Storage. *Small Methods* **2018,** *2* (6), 1700399.
8. Cardoso, V. F.; Correia, D. M.; Ribeiro, C.; Fernandes, M. M.; Lanceros-Méndez, S. Fluorinated Polymers as Smart Materials for Advanced Biomedical Applications *Polymers* [Online], 2018.
9. Zhang, C.-C.; Wang, Z.-K.; Yuan, S.; Wang, R.; Li, M.; Jimoh, M. F.; Liao, L.-S.; Yang, Y., Polarized Ferroelectric Polymers for High-Performance Perovskite Solar Cells. *Advanced Materials* **2019,** *31* (30), 1902222.
10. Li, H.; Wang, R.; Han, S.-T.; Zhou, Y., Ferroelectric polymers for non-volatile memory devices: a review. *Polymer International* **2020,** *69* (6), 533-544.
11. Surmenev, R. A.; Chernozem, R. V.; Pariy, I. O.; Surmeneva, M. A., A review on piezo- and pyroelectric responses of flexible nano- and micropatterned polymer surfaces for biomedical sensing and energy harvesting applications. *Nano Energy* **2021,** *79*, 105442.
12. Neese, B.; Chu, B.; Lu, S.-G.; Wang, Y.; Furman, E.; Zhang, Q. M., Large Electrocaloric Effect in Ferroelectric Polymers Near Room Temperature. *Science* **2008,** *321* (5890), 821.
13. Liu, P. F.; Wang, J. L.; Meng, X. J.; Yang, J.; Dkhil, B.; Chu, J. H., Huge electrocaloric effect in Langmuir–Blodgett ferroelectric polymer thin films. *New Journal of Physics* **2010,** *12* (2), 023035.
14. Lovinger, A. J., Poly(Vinylidene Fluoride). In *Developments in Crystalline Polymers—1*, Bassett, D. C., Ed. Springer Netherlands: Dordrecht, 1982; pp 195-273.
15. Tashiro, K.; Kobayashi, M., Structural phase transition in ferroelectric fluorine polymers: X-ray diffraction and infrared/Raman spectroscopic study. *Phase Transitions* **1989,** *18* (3-4), 213-246.
16. Furukawa, T., Ferroelectric properties of vinylidene fluoride copolymers. *Phase Transitions* **1989,** *18* (3-4), 143-211.
17. Lovinger, A. J., Polymorphic transformations in ferroelectric copolymers of vinylidene fluoride induced by electron irradiation. *Macromolecules* **1985,** *18* (5), 910-918.
18. Zhang, Q. M.; Bharti, V.; Zhao, X., Giant Electrostriction and Relaxor Ferroelectric Behavior in Electron-Irradiated Poly(vinylidene fluoride-trifluoroethylene) Copolymer. *Science* **1998,** *280* (5372), 2101-2104.
19. Xia, F.; Cheng, Z. Y.; Xu, H. S.; Li, H. F.; Zhang, Q. M.; Kavarnos, G. J.; Ting, R. Y.; Abdul-Sadek, G.; Belfield, K. D., High Electromechanical Responses in a Poly(vinylidene fluoride–trifluoroethylene–chlorofluoroethylene) Terpolymer. *Advanced Materials* **2002,** *14* (21), 1574-1577.
20. Chung, T. C.; Petchsuk, A., Synthesis and Properties of Ferroelectric Fluoroterpolymers with Curie Transition at Ambient Temperature. *Macromolecules* **2002,** *35* (20), 7678-7684.
21. Klein, R. J.; Xia, F.; Zhang, Q. M.; Bauer, F., Influence of composition on relaxor ferroelectric and electromechanical properties of poly(vinylidene fluoride-trifluoroethylene-chlorofluoroethylene). *Journal of Applied Physics* **2005,** *97* (9), 094105.
22. Zhu, L.; Wang, Q., Novel Ferroelectric Polymers for High Energy Density and Low Loss Dielectrics. *Macromolecules* **2012,** *45* (7), 2937-2954.
23. Liu, Y.; Aziguli, H.; Zhang, B.; Xu, W.; Lu, W.; Bernholc, J.; Wang, Q., Ferroelectric polymers exhibiting behaviour reminiscent of a morphotropic phase boundary. *Nature* **2018,** *562* (7725), 96-100.
24. Liu, Y.; Zhang, B.; Xu, W.; Haibibu, A.; Han, Z.; Lu, W.; Bernholc, J.; Wang, Q., Chirality-induced relaxor properties in ferroelectric polymers. *Nature Materials* **2020,** *19* (11), 1169-1174.
25. Liu, Y.; Chen, X.; Han, Z.; Zhou, H.; Wang, Q., Defects in poly(vinylidene fluoride)-based ferroelectric polymers from a molecular perspective. *Applied Physics Reviews* **2022,** *9* (3), 031306.
26. Tashiro, K.; Takano, K.; Kobayashi, M.; Chatani, Y.; Tadokoro, H., Structural study on ferroelectric phase transition of vinylidene fluoride-trifluoroethylene copolymers (III) dependence of transitional behavior on VDF molar content. *Ferroelectrics* **1984,** *57* (1), 297-326.

27. Green, J. S.; Rabe, J. P.; Rabolt, J. F., Studies of chain conformation above the Curie point in a vinylidene fluoride/trifluoroethylene random copolymer. *Macromolecules* **1986,** *19* (6), 1725-1728.
28. Tashiro, K.; Kobayashi, M., Vibrational spectroscopic study of the ferroelectric phase transition in vinylidene fluoride-trifluoroethylene copolymers: 1. Temperature dependence of the Raman spectra. *Polymer* **1988,** *29* (3), 426-436.
29. Kim, K. J.; Reynolds, N. M.; Hsu, S. L., Spectroscopic analysis of the crystalline and amorphous phases in a vinylidene fluoride/trifluoroethylene copolymer. *Macromolecules* **1989,** *22* (12), 4395-4401.
30. Reynolds, N. M.; Kim, K. J.; Chang, C.; Hsu, S. L., Spectroscopic analysis of the electric field induced structural changes in vinylidene fluoride/trifluoroethylene copolymers. *Macromolecules* **1989,** *22* (3), 1092-1100.
31. Jin Kim, K.; Reynolds, N. M.; Ling Hsu, S., Spectroscopic studies on the effect of field strength upon the curie transition of a VDF/TrFE copolymer. *Journal of Polymer Science Part B: Polymer Physics* **1993,** *31* (11), 1555-1566.
32. Kim, K. J.; Hsu, S. L., An infra-red spectroscopic study of structural reorganization of a uniaxially drawn VDF/TrFE copolymer in an electric field. *Polymer* **1994,** *35* (17), 3612-3618.
33. Faria, L. O.; Moreira, R. L., Infrared spectroscopic investigation of chain conformations and interactions in P(VDF-TrFE)/PMMA blends. *Journal of Polymer Science Part B: Polymer Physics* **2000,** *38* (1), 34-40.
34. Klein, R. J.; Runt, J.; Zhang, Q. M., Influence of Crystallization Conditions on the Microstructure and Electromechanical Properties of Poly(vinylidene fluoride−trifluoroethylene−chlorofluoroethylene) Terpolymers. *Macromolecules* **2003,** *36* (19), 7220-7226.
35. Mahdi, R. I.; Gan, W. C.; Majid, W. H. A., Hot Plate Annealing at a Low Temperature of a Thin Ferroelectric P(VDF-TrFE) Film with an Improved Crystalline Structure for Sensors and Actuators. *Sensors* **2014,** *14* (10).
36. Arrigoni, A.; Brambilla, L.; Bertarelli, C.; Serra, G.; Tommasini, M.; Castiglioni, C., P(VDF-TrFE) nanofibers: structure of the ferroelectric and paraelectric phases through IR and Raman spectroscopies. *RSC Advances* **2020,** *10* (62), 37779-37796.
37. Chapron, D.; Rault, F.; Talbourdet, A.; Lemort, G.; Cochrane, C.; Bourson, P.; Devaux, E.; Campagne, C., In-situ Raman monitoring of the poly(vinylidene fluoride) crystalline structure during a melt-spinning process. *Journal of Raman Spectroscopy* **2021,** *52* (5), 1073-1079.
38. Tashiro, K.; Kobayashi, M.; Tadokoro, H., Vibrational spectra and disorder-order transition of poly(vinylidene fluoride) form III. *Macromolecules* **1981,** *14* (6), 1757-1764.
39. Kobayashi, M.; Tashiro, K.; Tadokoro, H., Molecular Vibrations of Three Crystal Forms of Poly(vinylidene fluoride). *Macromolecules* **1975,** *8* (2), 158-171.
40. Cortili, G.; Zerbi, G., Chain conformations of polyvinylidene fluoride as derived from its vibrational spectrum. *Spectrochimica Acta Part A: Molecular Spectroscopy* **1967,** *23* (2), 285-299.
41. Gregorio, J. R.; Cestari, M., Effect of crystallization temperature on the crystalline phase content and morphology of poly(vinylidene fluoride). *Journal of Polymer Science Part B: Polymer Physics* **1994,** *32* (5), 859-870.
42. Gregorio Jr., R., Determination of the α, β, and γ crystalline phases of poly(vinylidene fluoride) films prepared at different conditions. **2006,** *100* (4), 3272-3279.
43. Cai, X.; Lei, T.; Sun, D.; Lin, L., A critical analysis of the α, β and γ phases in poly(vinylidene fluoride) using FTIR. *RSC Advances* **2017,** *7* (25), 15382-15389.
44. Milani, A.; Castiglioni, C.; Radice, S., Joint Experimental and Computational Investigation of the Structural and Spectroscopic Properties of Poly(vinylidene fluoride) Polymorphs. *The Journal of Physical Chemistry B* **2015,** *119* (14), 4888-4897.
45. Ma, W.; Zhang, J.; Chen, S.; Wang, X., β-Phase of poly(vinylidene fluoride) formation in poly(vinylidene fluoride)/poly(methyl methacrylate) blend from solutions. *Applied Surface Science* **2008,** *254* (17), 5635-5642.
46. Martins, P.; Lopes, A. C.; Lanceros-Mendez, S., Electroactive phases of poly(vinylidene fluoride): Determination, processing and applications. *Progress in Polymer Science* **2014,** *39* (4), 683-706.

47. Ren, J.-Y.; Ouyang, Q.-F.; Ma, G.-Q.; Li, Y.; Lei, J.; Huang, H.-D.; Jia, L.-C.; Lin, H.; Zhong, G.-J.; Li, Z.-M., Enhanced Dielectric and Ferroelectric Properties of Poly(vinylidene fluoride) through Annealing Oriented Crystallites under High Pressure. *Macromolecules* **2022,** *55* (6), 2014-2027.
48. Boccaccio, T.; Bottino, A.; Capannelli, G.; Piaggio, P., Characterization of PVDF membranes by vibrational spectroscopy. *Journal of Membrane Science* **2002,** *210* (2), 315-329.
49. Lin, Y.; Zhang, Y.; Zhang, F.; Zhang, M.; Li, D.; Deng, G.; Guan, L.; Dong, M., Studies on the electrostatic effects of stretched PVDF films and nanofibers. *Nanoscale Research Letters* **2021,** *16* (1), 79.
50. Tashiro, K.; Yamamoto, H.; Kummara, S.; Takahama, T.; Aoyama, K.; Sekiguchi, H.; Iwamoto, H., High-Electric-Field-Induced Hierarchical Structure Change of Poly(vinylidene fluoride) as Studied by the Simultaneous Time-Resolved WAXD/SAXS/FTIR Measurements and Computer Simulations. *Macromolecules* **2021,** *54* (5), 2334-2352.
51. Thakur, A.; Dam, S.; Dey, R.; Gangavarappu, A.; Hussain, S., Temperature Raman Studies of Freestanding and Flexible Thin Films of CdS-doped PVDF. *Polymer Composites* **2019,** *40* (7), 2662-2667.
52. Ji, Y.; Liu, J.; Jiang, Y.; Liu, Y., Analysis of Raman and infrared spectra of poly(vinylidene fluoride) irradiated by KrF excimer laser. *Spectrochimica Acta Part A: Molecular and Biomolecular Spectroscopy* **2008,** *70* (2), 297-300.
53. Wang, H.; Yang, X.; Zhao, Y.; Yan, C.; Wang, S.; Yang, H.; Wang, X.; Schultz, J. M., Preparation of gamma-PVDF with controlled orientation and insight into phase transformation. *Polymer* **2017,** *123*, 282-289.
54. Aliane, A.; Benwadih, M.; Bouthinon, B.; Coppard, R.; Domingues-Dos Santos, F.; Daami, A., Impact of crystallization on ferro-, piezo- and pyro-electric characteristics in thin film P(VDF–TrFE). *Organic Electronics* **2015,** *25*, 92-98.
55. Zhao, C.; Hong, Y.; Chu, X.; Dong, Y.; Hu, Z.; Sun, X.; Yan, S., Enhanced Ferroelectric Properties of P(VDF-TrFE) Thin Film on Single Layer Graphene Simply Adjusted by Crystallization Condition. *Materials Today Energy* **2021**, 100678.
56. Wongwirat, T.; Zhu, Z.; Rui, G.; Li, R.; Laoratanakul, P.; He, H.; Manuspiya, H.; Zhu, L., Origins of Electrostriction in Poly(vinylidene fluoride)-Based Ferroelectric Polymers. *Macromolecules* **2020,** *53* (24), 10942-10954.
57. Zhu, Z.; Rui, G.; Li, R.; He, H.; Zhu, L., Enhancing Electrostrictive Actuation via Strong Electrostatic Repulsion among Field-Induced Nanodomains in a Relaxor Ferroelectric Poly(vinylidene fluoride-co-trifluoroethylene-co-chlorotrifluoroethylene) Random Terpolymer. *ACS Applied Materials & Interfaces* **2021,** *13* (35), 42063–42073.
58. Bargain, F.; Thuau, D.; Hadziioannou, G.; Domingues Dos Santos, F.; Tencé-Girault, S., Phase diagram of poly(VDF-ter-TrFE-ter-CTFE) copolymers: Relationship between crystalline structure and material properties. *Polymer* **2021,** *213*, 123203.
59. Bargain, F.; Thuau, D.; Panine, P.; Hadziioannou, G.; Domingues Dos Santos, F.; Tencé-Girault, S., Thermal behavior of poly(VDF-ter-TrFE-ter-CTFE) copolymers: Influence of CTFE termonomer on the crystal-crystal transitions. *Polymer* **2019,** *161*, 64-77.
60. Hafner, J.; Benaglia, S.; Richheimer, F.; Teuschel, M.; Maier, F. J.; Werner, A.; Wood, S.; Platz, D.; Schneider, M.; Hradil, K.; Castro, F. A.; Garcia, R.; Schmid, U., Multi-scale characterisation of a ferroelectric polymer reveals the emergence of a morphological phase transition driven by temperature. *Nature Communications* **2021,** *12* (1), 152.
61. María, N.; Le Goupil, F.; Cavallo, D.; Maiz, J.; Müller, A. J., Effect of the TrFE Content on the Crystallization and SSA Thermal Fractionation of P(VDF-co-TrFE) Copolymers. *International Journal of Molecular Sciences* **2022,** *23* (18), 10365.
62. Yagi, T., Heat of Fusion and Crystallization Kinetics of Poly(trifluoroethylene). *Polymer Journal* **1980,** *12* (1), 9-15.
63. Koga, K.; Ohigashi, H., Piezoelectricity and related properties of vinylidene fluoride and trifluoroethylene copolymers. *Journal of Applied Physics* **1986,** *59* (6), 2142-2150.
64. Meng, N.; Zhu, X.; Mao, R.; Reece, M. J.; Bilotti, E., Nanoscale interfacial electroactivity in PVDF/PVDF-TrFE blended films with enhanced dielectric and ferroelectric properties. *Journal of Materials Chemistry C* **2017,** *5* (13), 3296-3305.

65. Kim, K.; Lee, S.; Nam, J.-S.; Joo, M.; Mikladal, B.; Zhang, Q.; Kauppinen, E. I.; Jeon, I.; An, S., Highly Transparent and Mechanically Robust Energy-harvestable Piezocomposite with Embedded 1D P(VDF-TrFE) Nanofibers and Single-walled Carbon Nanotubes. **2023,** *33* (14), 2213374.
66. Ohigashi, H.; Koga, K., Ferroelectric Copolymers of Vinylidenefluoride and Trifluoroethylene with a Large Electromechanical Coupling Factor. *Japanese Journal of Applied Physics* **1982,** *21* (8A), L455.
67. Osswald, S.; Mochalin, V. N.; Havel, M.; Yushin, G.; Gogotsi, Y., Phonon confinement effects in the Raman spectrum of nanodiamond. *Physical Review B* **2009,** *80* (7), 075419.
68. Lin-Vien, D.; Colthup, N. B.; Fateley, W. G.; Grasselli, J. G., CHAPTER 3 - Halocompounds. In *The Handbook of Infrared and Raman Characteristic Frequencies of Organic Molecules*, Lin-Vien, D.; Colthup, N. B.; Fateley, W. G.; Grasselli, J. G., Eds. Academic Press: San Diego, 1991; pp 29-44.